2022
9(1), 47-60

Journal of
MATERIALS NANOSCIENCE

A comprehensive review on functionalized Hydroxyapatite nanostructures based gas sensors for environmental pollutant monitoring

N. Manjubaashini, G. Radha, S. Balakumar*

National Centre for Nanoscience and Nanotechnology, University of Madras, Chennai – 600025. India

Submitted on: 17-Nov-2021, Accepted and Published on: 15-Feb-2022

Review Article

ABSTRACT

The utilization of advanced sensing techniques for detecting and monitoring toxic gases in industry and the environment is a predominant action. For such applications, the sensor material should possess higher sensitivity, faster detection, and real-time operation. Mostly, metal oxides (MOs) are preferred for gas sensing purposes owing to their excellent sensing property, wide band-gap, electrical conductivity, and high surface reactivity. But, the same MOs lag in many perspectives like low selectivity, higher operating temperature (> 400 °C), more power consumption, and reduced stability. Since more emphasis is given to materials that operate at room temperatures like nano-hydroxyapatite (nHAp), it's a bio-ceramic material used for chemical gas sensing. The nHAp is a matrix of rich calcium (Ca^{2+}) and phosphate (PO_4^{3-}) ions. In chemical gas sensors, the nHAp possess significant properties like large surface phosphate-hydroxide (P-OH) groups, ionic conductivity, porous nature, and ion exchange capability for effective gas molecule interaction. In this profound review, we discussed the nHAp structure with different fabrication techniques for gas sensing. Particularly, functionalized nHAp with MO and polymers were focused and their stability, sensitivity, selectivity, and adsorption rate are presented along with different mechanisms. Existing challenges and future perspectives of nHAp material are also highlighted.

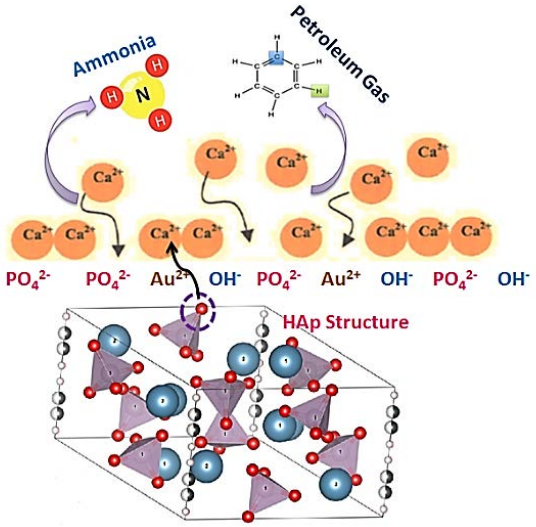

Keywords: Nano-hydroxyapatite, Gas Sensing, Bio-ceramic, Polymer, Sensitivity, Conductivity

INTRODUCTION

In the present situation, more attention has been focused on health and environment-related research challenges. In particular, owing to the increasing hazardous pollutants from industries, transportation, agriculture, and commercial products; the air, water, and soil are contaminated through the emission of poisonous gases.[1] Consequently, high demand is created for smart sensors with enhanced accuracy with excellent selectivity and sensitivity[2] towards environmental remediation. The role of gas sensors has a wide market in the field of transportation, telecom, aerospace, automobile products, medical equipment, and industries.[3] Additionally, the rapid increase of various industries may produce hazardous gases which cause health defects. The overwhelming production of carbon and carbon-based gases like CO, CO_2 are very dangerous for human health.[4] Based on industrial waste regulations, the demand for highly reliable and accurate sensors has become increased for human survival.[5] For this reason, a more reliable and efficient gas-sensing system is important to detect environmentally harmful gases and volatile organic compounds (VOC), hydrogen peroxide, rare-earths, petroleum gases, and other alcoholic compounds.[6] After a certain level of exposure, these substances may cause eye, skin, and stomach irritations addition to liver, brain and respiratory problems.[7] Hence, the detection of these gases and vapors at lower concentrations is very essential for environmental and human health welfare.

The rapidly emerging MO-based nanomaterials show enhanced sensitivity, excellent selectivity, and processability as promising parameters for the development of room temperature sensors.[8] Transition MO like ZnO,[9–11] TiO_2 [12–14] and SnO_2[15] have been used for H_2, NO_x, CH_4, and CO_2 sensing.[16–20] Furthermore, materials such as TiO_2, doped with CuO and La_2O_3, are used for CO sensing for combustion applications. The SnO_2 nanoparticles (NPs) doped nickel for CO gas sensor was developed by Zhou et

*Corresponding Author: Prof. S. Balakumar, Director, National Centre for Nanoscience and Nanotechnology, University of Madras, Chennai – 600025. India

Email: balasuga@yahoo.com

URN:NBN:sciencein.jmns.2022.v9.293

ISSN: 2394-0867
https://pubs.thesciencein.org/jmns

al., 2018 had a superior sensing response compared to SnO_2 and Zn doped SnO_2.[21] Rizi et al., 2019 developed a ceramic nanocomposite (CNC) made of SnO_2/Ag_2O to detect H_2 gas.[22] Tong et al., 2019 prepared cobalt-TiO_2 Nanotubes by anodization followed by immersion approach.[23] Yin et al., 2019 revealed a sensor with greater selectivity, stability, and reproducibility, with a response value of 199.16s for 50 ppm H_2S, showing a 7.6-fold improvement over un-doped sensors.[24] Awfully, the above-discussed MO-based gas sensors suffer from important parameters like instability at higher temperature operating conditions, non-optimal temperature range, less dielectric nature, insufficient binding sites, and may cause environmental hazards.[25] Thus, to rectify the problems related to MO-based gas sensors, naturally occurring and eco-friendly nano-hydroxyapatite (nHAp) materials were introduced. Predominantly, the HAp materials are used widely for biomedical applications like bone tissue formation with different substituents like sulphate[26], magnesium[27], Iron oxide[28], silver ion[29], graphene nanosheets[30], Copper ions[31], PMMA[32], etc., for orthopedic and dental applications. Since, nHAp is being used in many biomedical field; there are numerous articles were published related to biomedical applications. But for gas sensing applications, the nHAp has various significant properties like larger active surface sites with high surface area and porous nature by tuning their electrical and structural properties, also the nHAp would act as good dielectric material.[1,6] Figure. 1 shows the sensing ability of nHAp for various organic contaminants, and the publications of nHAp based on the gas sensor from 2015 to 2021. Herein, we present a comprehensive review of nHAp and its composites for gas sensing applications. In addition, the physical, chemical, structural, electronic, and electrochemical properties of nHAp were also discussed in detail. We also focused on the various gas detecting performance of nHAp in combination with various metal ions, conductive polymers, and carbonaceous nanostructures through different principles and mechanisms. Additionally, the fabrications of nHAp based composite structures by different coating techniques were also discussed. Moreover, this review article comprises the challenges of the nHAp gas sensor along with future perspectives.

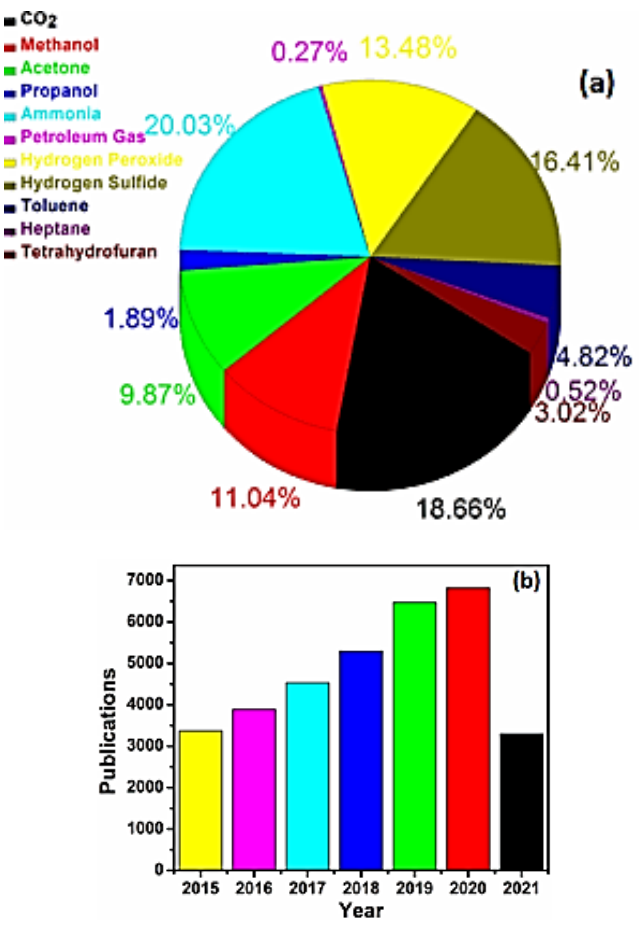

Figure 1. (a) Comparison on various gas analyte sensing, (b) Number of articles published based on nHAP in the last 5 years.

Overview of nHAp for Sensing

The better properties of nHAp, as well as its ability to receive plenty of anionic and cationic variants, make it possible to use in a variety of applications.[33] The microstructure of HAp, such as particle size, shape and distribution, porosity, and crystallinity, influences its effectiveness.[34] The chemical makeup of nHAp is similar to bone tissues, making it suitable for biomedical applications. Also, nHAp is widely used in many applications, including fluorescent lamps, fuel cell materials, and pollutant adsorption.[35] Due to its porous and cage-like structure, wide surface area, P-OH group that interacts with the sensing molecule, and ionic conductivity,[36,37] nanocrystalline HAp ($Ca_{10}(PO_4)_6(OH)_2$) has been successfully used as a promising candidate meant for fabricating gas and chemical sensor devices.[38] The two principal elements that are present in nHAp are calcium and phosphate, which also contain hydroxide with hydrogen atom connected to oxygen as a chemical interaction which includes electron exchange.[36] Because of its high sensitivity, fast response, strong selectivity, stability, porous nature, considerable electrical characteristics, and absorption capacity, NanoHAp behaves like an effective sensing material. HAp crystal structure is made up of a different combination of ions, including PO_4^{3-}, OH^-, and Ca^{2+} and it has a high ion exchange capacity. Various divalent metal cations, such as Sr^{2+}, Mg^{2+}, Cd^{2+}, Mn^{2+}, Pb^{2+}, Co^{2+}, Ba^{2+}, Ni^{2+}, and Zn^{2+}, can easily replace the Ca^{2+} ions in the crystal. It is feasible to modify the OH^- radicals with Cl^- and/or F^- anions and substitute PO_4^{3-} groups with carbonate and sulfite ions.[39]

The electrical properties of nHAp and doped nHAp were used for various gas sensing applications. Generally, the nHAp has a constant high dielectric conductivity. The dielectric properties of nHAp were studied by permeability and permittivity against frequency.[40] The frequency dependence over sensing material alone is not sufficient for gas sensing application. The nHAp lacks electron transfer and conductivity properties, hence the material should dope with materials like MOs, conductions polymers, and graphene derivatives.[34]

PROPERTIES AND PREPARATION TECHNIQUES OF nHAP

The nHAp is one of the thermodynamically stable materials.[41] Each unit cell of stoichiometric nHAp contains 10 Ca^{2+}, 6 PO_4^{3-} and 2 OH^- groups. In which OH^- is placed at the unit cell sides, 10 Ca^{2+} ions have two different subsets of Ca^{2+} (1) and (2).[42] The 4 Ca^{2+} ions occupy Ca^{2+} (1) positions and 6 O_2 atoms are placed at Ca-O octahedron mid-point. Further, the PO_4^{3-} tetrahedral forms a crystalline network of nHAp and affords stability.[32] When OH^- is coupled with 2 Ca^{2+} (2) ions on the crystalline HAp surface, the OH^- radicals may be unoccupied at specific points.[43] When PO_4^{3-} is on the crystal's surface, H_2O forms a hydrogen bond with it. The HAp is more stable than other calcium orthophosphates at physiological pH (7.2 to 7.4).[44] Wet chemical, chemical precipitation, sol-gel, solvothermal, and hydrothermal techniques can be used to prepare HAp. The most convenient and widely utilized method of precipitation is based on a wet chemical process.[45] Microwave technique is also the best option since it is environment amicable, safer, and easier.[46,47] In addition, the hydrothermal method operates at high temperatures with optimum pressures is often utilized. In addition, the material's elemental and chemical composition could be successfully adjusted.[48,49] The gas sensing properties for various materials were discussed in Table. 1.

Table 1. Morphology and sensing features of different materials used for the detection of various gas sensing.

Sensor Material	Sensing Material	Operating Temperature	Response/Recovery time (s)/Detection Limit	Ref. No.
$ZnFe_2O_4$	NO_2	600 °C	195s/17s/400 ppm	50
Silver nanoparticles (Ag NPs)/rGO	NH_3	-	76s/84s/250 ppb	51
Cerium Oxide	O_2	700 °C	10s/10^5-10^3 Pa	41
ZnO Nanoflowers	CH_3OH	300 °C	48s/25s/100 ppm	52
p-TiO_2	Ethanol	320 °C	120s/60s/50 ppm	53
SnO_2 Nanowires	Ethanol	400 °C	10s/14s/50 ppm	54
CuO Nanosheets	H_2S	240 °C	4s/9s/1.2 ppm	55
HAp thick films	CO_2	165 °C	3x10^{11} ions/cm^2	56
Gold (Au)-HAp	NH_3	RT	20s/25s/200x10^{-6}	57
HAp	CO	125 °C	900 ppm	44

NANO-HAP BASED GAS SENSOR

Ammonia (NH_3) Sensing

Researchers have created HAp-based composites with various polymers with conducting nature such as polyaniline (PANI) and polypyrrole (PPy).[58,59] To improve the sensitivity of NH_3, PPy and PANI were combined with HAp and formed as PPy/HAp and PANI/HAp composites for testing NH_3 sensitivity, response, recovery time, and selectivity (Figure. 3). A chemical oxidative polymerization approach was used to make PPy and PANI at room temperature. The tubular like HAp were made *via* electrochemical deposition process with the help of a cation exchange membrane, then stewed for 7 days at 50 °C.[60] Mechanical mixing was used to create the composites PPy/HAp and PANI/HAp.[61] The tubular HAp sensing mechanism of NH_3 was proposed in Figure. 2. In the NH_3 sensing mechanism, the HAp is tuned as an n-type semiconductor with decreased electrical resistance.[62]

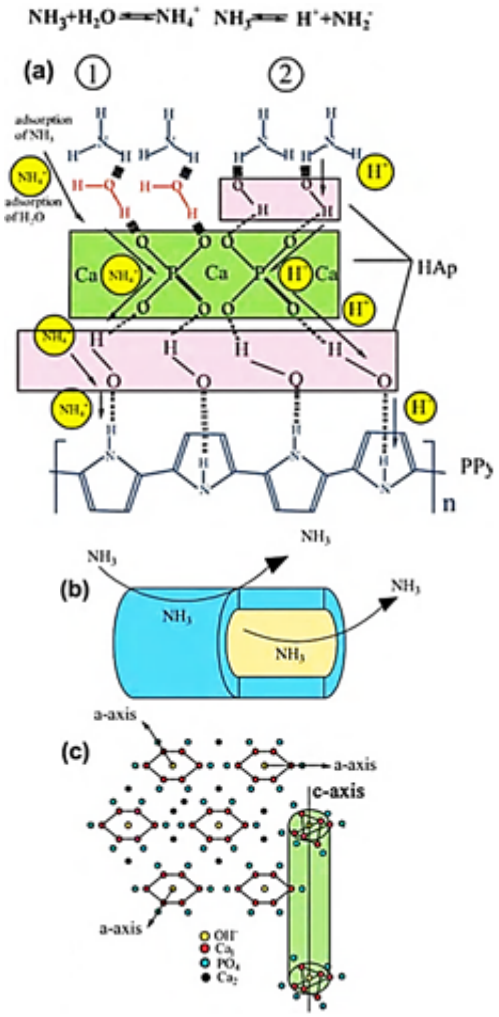

Figure 2. Mechanism of ammonia sensing by HAp composites.[49]

The three-dimensional (3D) network structure of the HAp was effectively determined for NH_3 sensing.[63] The gas sensor was made using an electrochemical deposition process on an indium tin oxide (ITO) glass (Figure. 4A).[53] The gas system will be installed along with the vacuum-sealed unit, the auxiliary, and the working electrode of the workstation committed to electrode B and electrode A. The gas input and outlet are both available in the chamber. The vacuum pump was used to evacuate the chamber before the test, and the vacuum gauge linked to the chamber was used to measure the pressure inside the gas chamber. Gas sampling bags were used to prepare 100-1000 ppm ranges of NH_3

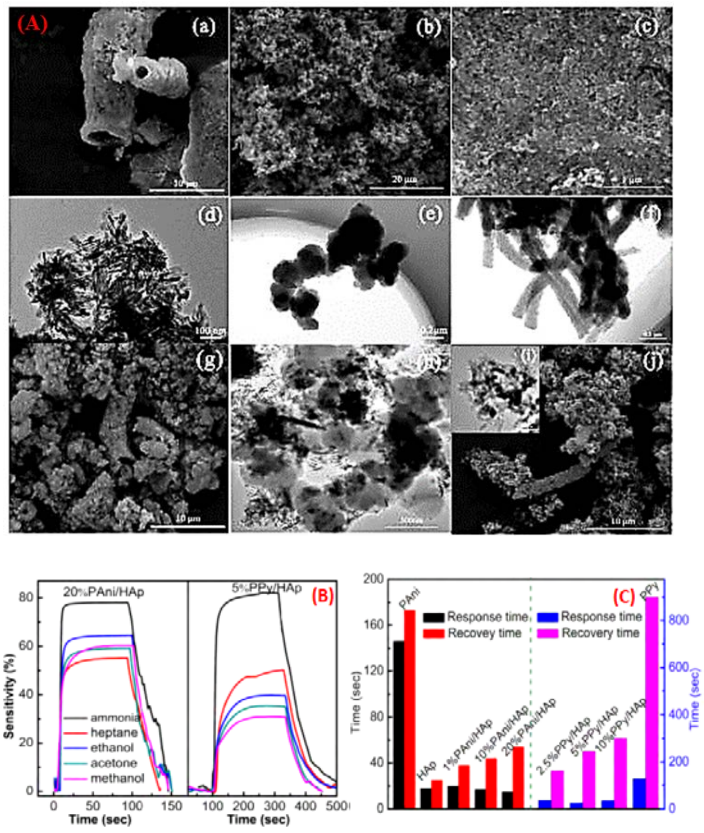

Figure 3. (A) SEM and TEM micrographs of pure and composites, (B) Sensitivity curve of PANI/HAp composite, (C) Response and recovery plot for pure and composites against ammonia.[49]

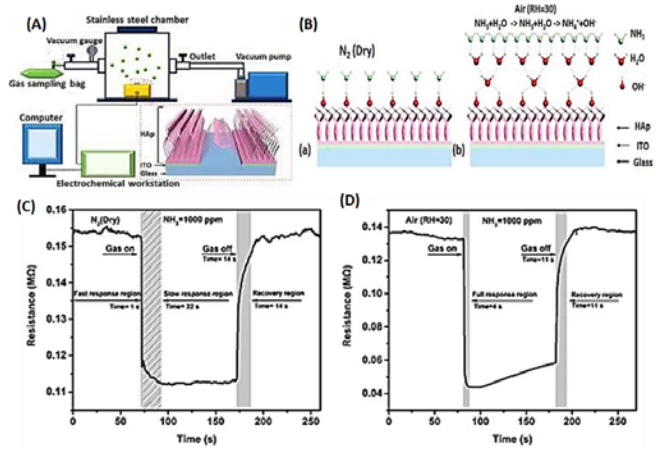

Figure 4. (A) Prototype model for gas sensor; (B) Mechanism of HAp film sensor at different conditions; (a) N_2 (dry), (b) air (RH≈30); (C) Resistance behavior of HAp film to sense NH_3 gas at different conditions N_2 dry and air (RH≈30).[64]

gas and attached to the seat unit for analysis with 83.7 % yield (Figure. 4C). The sensing method of HAp film was obtained. First, in the presence of N_2, the -OH ions were adsorbed and their response site for capturing NH_3 ions on the surface of the HAp.[65] In a nutshell, the $^-$OH ions adsorb NH_3 molecules on the HAp surface and are exposed to N_2 (dry).[66] The H_2O molecular on the surface interact with $^-$OH ions and NH_3 molecules and form H_2 bond in the presence of air (RH=30) (Figure. 4B).[64]

Researchers developed gold (Au) modified hydroxyapatite (HAp) for sensing NH_3. The tube-like HAp structure was developed by cation exchange membrane and the gold nanoparticles prepared by hydrothermal technique were further made like a paste with ionized water.[67] The Au-HAp modified film fabricated by ceramic tube with paste.[57] The following samples (HAp, 2AuHAp, 5AuHAp, and 10AuHAp) were examined for their reactions to NH_3 gas. The pure HAp morphology is like a tube with 2.5 µm dia. The self-assembly of nanorods is thought to be responsible for the structure's shape. The morphology of 5AuHAp is shown in Figure 5B(b), is identical to that of HAp after the addition of Au. Figure 5B(c) and 5B(d) depict the outside and inner surfaces of pure tube-like HAp. Both the surfaces are rough, with needle and tabular morphology. The agglomerates in 5AuHA (Figure. 5B(e)) are made of nanorods. At room temperature, both HAp and Au-HAp have a better sensitivity to a variety of gases, with NH_3 having the strongest reaction. With a 90% response value for NH_3 concentration of $2000x10^{-6}$ and 70.8% at an NH_3 concentration of $50x10^{-6}$, the AuHAp with 5% Au has good gas absorbing characteristics (Figure. 6). The Au nanoparticles show unusual tube-like morphology of HAp, and major features contribute to the high responsiveness and selectivity to NH_3.

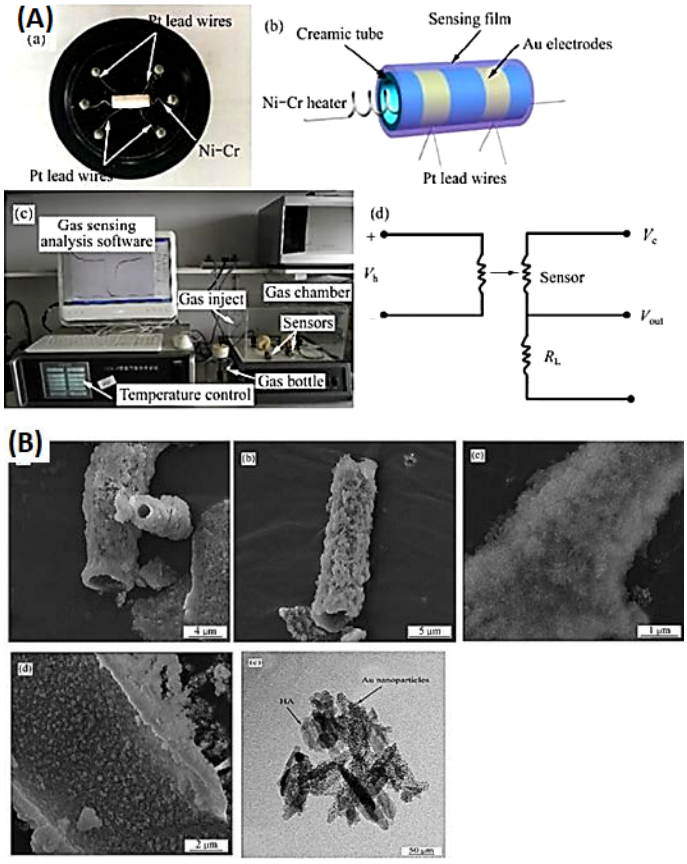

Figure 5. (A) (a) Gas sensing device, (b) Design of ceramic tube, (c) Gas-sensing system (CGS-8 intelligent), (d) Analysis schematic; (B)SEM micrographs (a) HAp, (b) Au−Hap, (c) Outer surface of HAp (d), Inner surface of Hap, (e) TEM image of Au−HAp.[57]

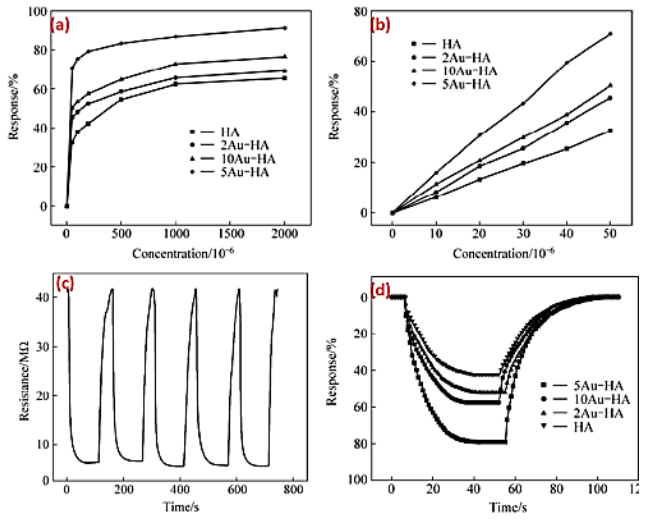

Figure 6. (a and b) Response curve of HAp and Au-HAp with varying concentrations of NH_3 gas at room temperature, (c) Sensor resistance of 5Au−HA versus time, (d) Response curve of HAp, Au−HAp (200×10^{-6}) NH_3 at room temperature.[57]

The NH_3 gas detection was examined by nanocomposite films made by nanosized HAp and cellulose nanofibril (CNF).[68,69] The freeze-drying process determines the film porosity (Figure. 7a(A)). The HAp pore size, gradient, and particle rearrangement over freeze-drying direction cause H_2O molecule formation around CNFs.[70,71] The CNF film (Figure. 7b) shows more closely packed net structures of bundles and solitary CNFs, whereas the HAp material was uniformly dispersed, comparatively agglomerated, and showed differentially sized particles (Figure 7a(B)). Furthermore, in the case of the 5HCNF50 composite (Figure. 7b(C)), the surface of the net-like CNFs surface was coupled with longitudinal-type HAp particles, whereas in 10HCNF50 composite, agglomeration occurs at a precise area due to increased HAp concentration. Thus, HAp with microporous structure, less density, homogeneously dispersed and longitudinally-shape shows high sensitivity of 75% for NH_3 gas and detection limit (LoD) of 5 ppm at 25°C and with decreased response and recovery time 210 and 30 s respectively (Figure. 7c).

The HAp-(Graphene) GR's gas sensing capabilities include responses to a variety of gases like ammonia, acetone, ethanol, methanol, tetrahydrofuran, toluene, and heptane (Figure. 8B). [72] Around 35.7 %, 41.6 %, 38.4 %, 69.5 %, 36.5 %, 49.6 %, and 35.5 % are the response for sensitivities, accordingly. The material shows higher sensitivity to NH_3 along with strong selectivity. The differences in gas sensing performance between cHAp-GR and bHAp-GR composites are mostly due to structural and morphological variations. The bHAp/GR composites have significant small crystals and porous nature, have a substantially higher response with increased systematic sensitivity to NH_3 than the cHA-GR composites; thus, the gas sensing features of HAp-GR composites may be easily modified by controlled synthesis. The chemical precipitation process produces needle-shaped HAp which linked to the layers of graphene in the cHA/GR composites (Figure. 8A). Figure. 8A(d) and 8A(f) demonstrate that, after 15

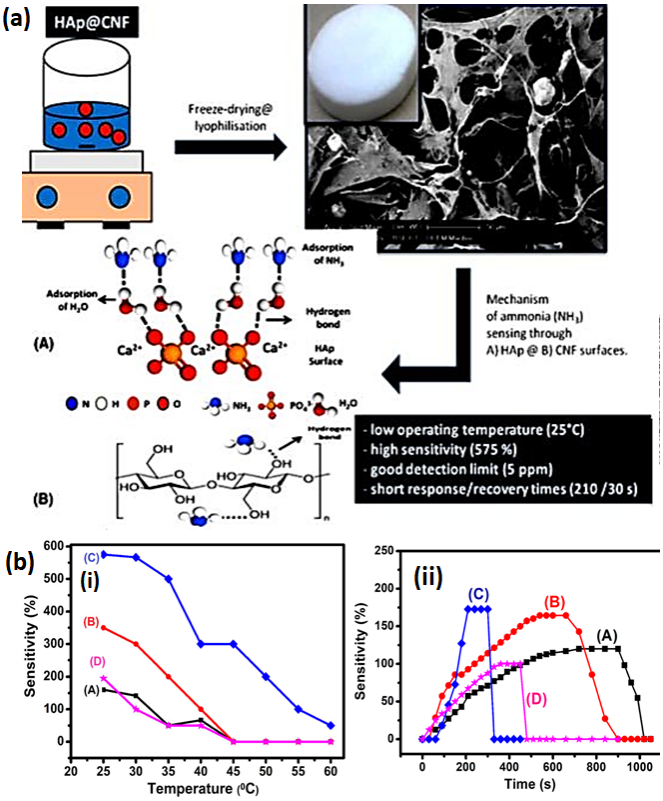

Figure 7. (a) Representation NH_3 sensing mechanism by HAp structure with cellulose nanofibrils, (b) (i) Sensitivity of pure and nanocomposite films against NH_3 gas based on temperature; (ii) Recovery time of NH_3 in ambient air at room temperature.[71]

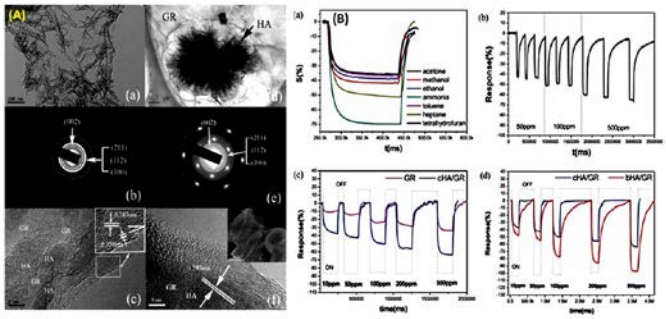

Figure 8. (A) HRTEM images for HAp-graphene composites; (a, b, c) Chemical precipitation method, (d, e, f) biomimetic method, (B) (a) Response and recovery time of cHA-GR composites at varying concentrations, (b) cyclic stability of cHA-GR to NH_3 at various concentration, (c) response and recovery time of fGR and cHA-GR to NH_3 at various concentration, (d) sensing characteristics of cHA-GR and bHA-GR composites against NH_3 at various concentration.[73]

days of immersion in 1.5 SBF, HAp microspheres with a diameter of 3 m are generated and enveloped for network formation of graphene. The linked and porous architecture of HAp agglomerates may be recognized.[73]

Researchers discovered TiO_2-modified HAp as a possible NH_3 sensor material at lower temperatures.[74] Wet chemical technique was used to make nano-ceramic HAp. Mechanical mixing of TiO_2 with HAp powder is used to blend TiO_2-HAp. The typical screen-printing procedure is used to create thick films from such blended materials. The sensing capabilities of commercial HAp,

commercial TiO_2, and composite thick films were investigated using gas sensing analyses.[75] Thick films resistance in the air (R_a) and gas (R_g) is determined.[48] The temperature of the sensor substrate (thick film) is kept between 350 °C and 30 °C for determining R_{gas} and R_{air} separately, and then the sensitivity is computed. The maximal sensitivity at a given temperature is then determined by drawing a graph of sensitivity% for temperature variant. The operating range of the sensor thick film is determined by the temperature at which greater sensitivity is observed. The sensing performance of 1 wt% TiO_2 blended HAp thick films have displayed high sensitivity, faster response, and recovery time for the fixed concentration of NH_3 (10 ppm) in comparison with other composites. It also possesses a higher uptake capacity of 900 ppm of NH_3 vapors in ambient conditions (Figure. 9). Thus, it can be utilized for commercial applications as an efficient sensor substrate for NH_3 in sensor devices.[65]

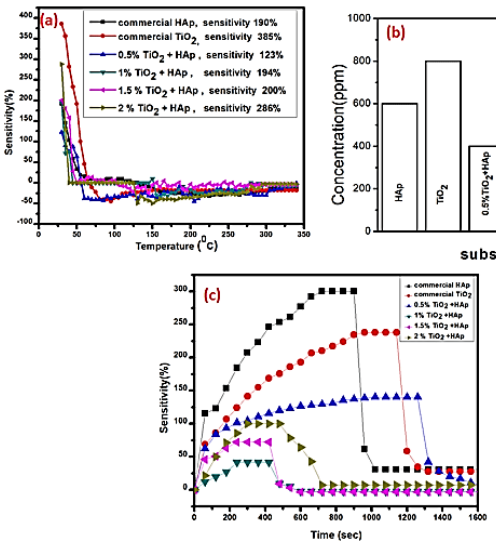

Figure 9. (a) Gas response with temperature variants for NH_3 gas at 10 ppm, (b) Ammonia gas sensing capacity with varying concentration for commercial HAp, commercial TiO_2, and composites, (c) Percentage of sensitivity for commercial HAp, commercial TiO_2, and composites.[75]

Tubular HAp has a 3D and semi-crystalline nature than rod-like HAp. Tubular HAp material has a faster response and recovery than rod-shaped HAp material. The HAp sensing mechanism involves oxygen interaction with gas molecules to target gases.[76] The results show ion-exchange sulfonic ions permit Ca^{2+} to pass across the membrane, suggesting a plausible creation process for tube HAp. The defect domains and hydrophobic nature would prevent Ca^{2+} from passing through and allow HAp crystals to nucleate and develop (Figure 10A(a)). The membrane is then covered in HAp crystals for the most part, except the domains, where Ca^{2+} ions do not penetrate. Long nanosheets are formed when HAp crystals develop preferentially along the c-axis. The nanosheets combined with specific orientation for cluster formation to minimize their surface energy (Figure. 10A(b)).[77] As the clusters get thicker, Ca^{2+} ion penetration becomes more difficult, thus Ca^{2+} ions are constantly

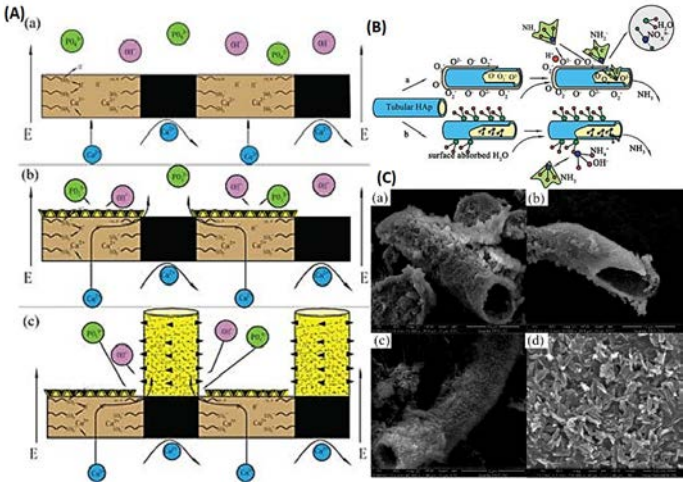

Figure 10. (A) The synthesis process of tubular HAp; (B) Sensing mechanisms of tubular HAp against ammonia; (C) Morphology of HAp by different methods; (a-c) membrane assisted electrochemical deposition method, (d) hydrothermal method.[76]

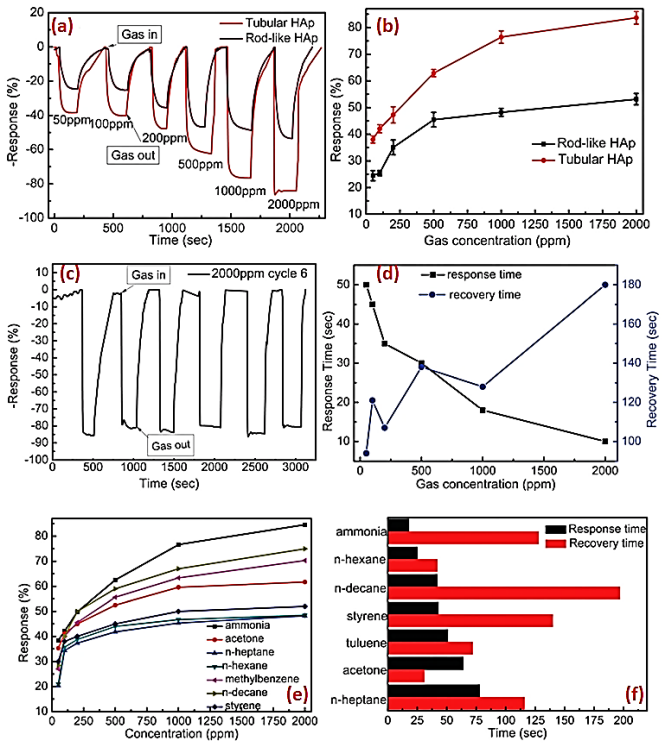

Figure 11. (a) Response curve based on time variation, (b) response curve based on ammonia concentration, (c) Response curve for continuous cycles of 2000 ppm, (d) recovery time based on gas concentration, (e) Response of tubular HAp based on concentrations for various gases, (f) recovery time based on different gases.[76]

transported to the edges of those domains, which acts as a calcium ion spring, allowing tubular HAp (Figure. 10A(c)). The electrochemically deposited HAp with tubular morphology of 2.5 mm diameter and 20 mm length (Figure. 10C (a–c)). Figure 10d shows hydrothermally synthesized HAp with rod morphology. Tubular HAp sensors respond to NH_3 which is faster than rod

morphology sensors. The HAp tubular morphology shows 84.58% response to NH_3 for 2000 ppm within10 sec (Figure. 11).[78]

H_2S Sensing

The HAp and its composite were determined for H_2S detection with tubular HAp morphology and acidithiobacillusferrooxidans (At. f) (Figure. 12B). H_2S gas is toxic to the environment, combustible, corrosive nature, and foul-smelling acid gas that is created in coal mines, petroleum fields, sewage, and decrease natural gases. Both the human body and the ecosystem are severely harmed.[79,80] The At. F bacterial which is gram-negative used in the desulphurization of coal and gases.[81] By combined At. f with HAp will increase the sensitivity towards effective gas detection.[82] At.f was grown traditionally on 9K medium with a pH of 2. The flask was incubated at 30 °C for 8 h on a rotating shaker. The centrifugation process was used to gather and wash

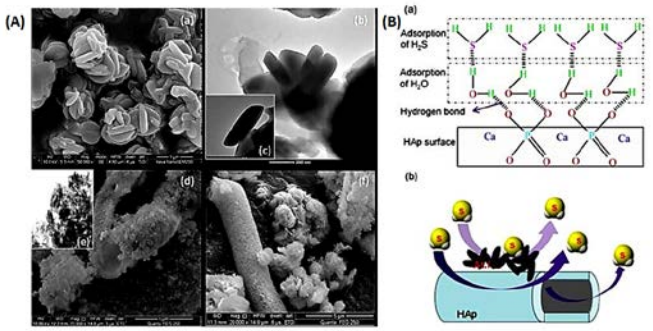

Figure 12. (A) Morphology of HAp with and without bacterial medium; **(**B) Mechanism of H_2S gas detection (a) HAp surface, (b) At.f-HAp composite.[79]

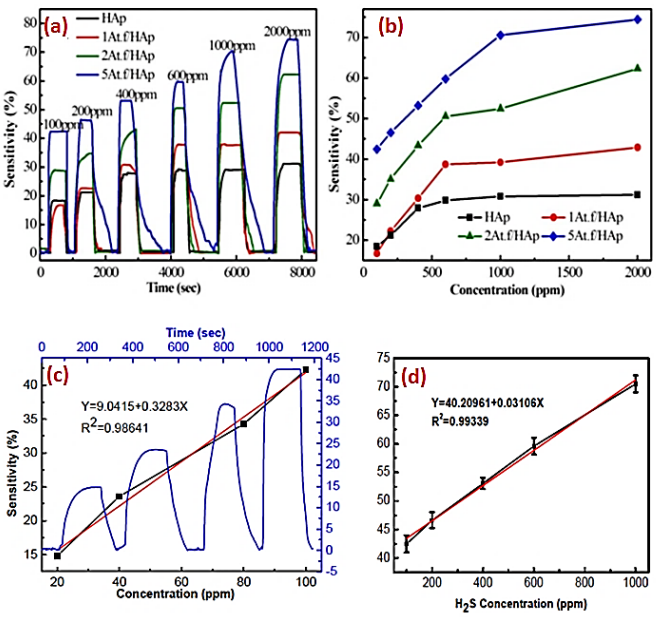

Figure 13. The sensitive curve for H_2S gas based on At.f-HAp composites (a) varying concentrations based on time, (b) Varying concentrations from 20-100 ppm (c, d) sensitivity linear fit of At. f-HAp for H_2S detection. [79]

the living bacteria. At. f with different concentrations were combined with HAp. At.f microstructure shows rod morphology (Figure 12A (a-c)). The tube is made up of clusters of 10-20 nm diameter nanorods with a length of roughly 100 nm (Figure. 12A (d-e)). Physically, At. f and HAp were mixed. (At. f) improved the sensing characteristics of At.f and tubular HAp composites for H_2S sensing and their significance. Compared to HAp, the At.f-HAp composite shows 2.5 times increased sensitivity (Figure. 13). At.f-HAp composites have a short and consistent response and recovery curve. The morphology and concentration of At.f. were proposed to be strongly related to the composites' H_2S sensing mechanism. The At. f/HAp composites have a lot of potential for sensing H_2S gas.[83]

CO_2 Sensing

Thick sheets of HAp-cobalt composite for CO and CO_2 detection were considered. Using a screen-printing process, HAp-Co powder is prepared as thick film. A wet chemical technique was used to make nano-ceramic HAp. Screen printing was used to create ion-exchanged nanoceramic Co-HAp powders. Ag^{7+} ions with a power of 100 MeV are used in ion irradiation. The samples are bombarded with $3x10^{11}$ to $3x10^{13}$ ions/cm^2 of ion influence. The HAp-Co films gas detection features are improved using rapid heavy ion irradiation. In the repeatability test, the composite was confirmed at (135 °C) lower operating temperatures for CO and CO_2 detection. When compared to pristine HAp $3x10^{11}$ ions/cm^2, the response recovery time for co-doped HAp $3x10^{11}$ ions/cm^2 is observed to be small (Figure. 14). Furthermore, for CO and CO_2 gases, the absorption range for HAp-Co is $3x10^{11}$ ions/cm^2 at different concentrations.[84]

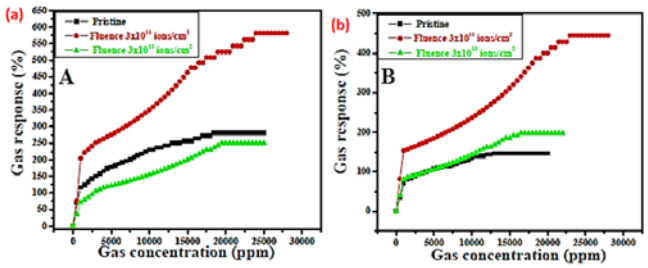

Figure 14. Sensitivity and response curve of pure and ion irradiated HAp-CO (a) CO gas, (b) CO_2 gas.[84]

The controlled structure and active surface of HAp at ambient conditions were prepared by one-step mechano-chemical treatment.[85,86] The spherical morphology is obtained for raw and mechano-chemically processed HAp (Figure. 15A). The mechanochemically treated samples were agglomerates as close-packed particles compared to raw HAp. The HAp surface activation of HAp will be demonstrated as follows; (i) The treated HAp has enhanced radical formation with strong basicity, the raw HAp surface oxygen vacancy occupied by PO_4^{3-} ions; (ii) Although radical production and basicity increased on treated HAp activity, CO_3^{2-} addition and HPO_4^{2-} synthesis occurred on both the –OH and PO_4^{3-} sites under high mechanical stress can be

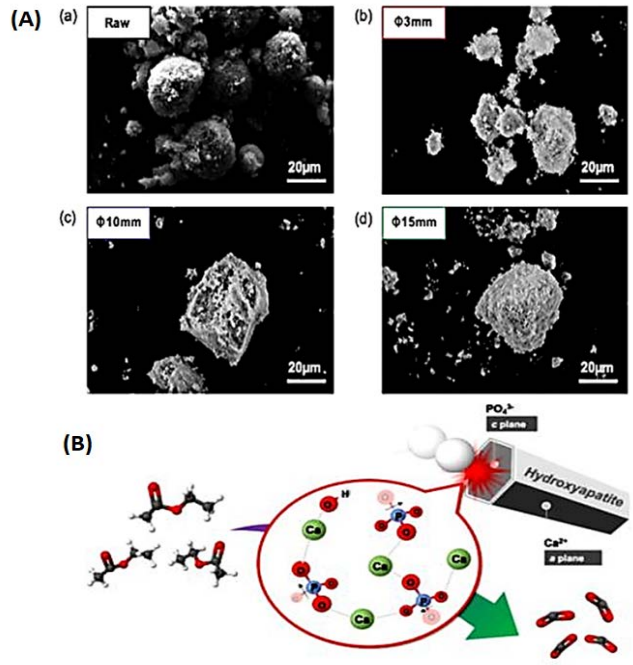

Figure 15. (A) Structure of raw and treated HAp, (B) Process of catalytic oxidation of VOC by mechano-chemical tailored HAp towards 100% CO_2/ CO conversion.[87]

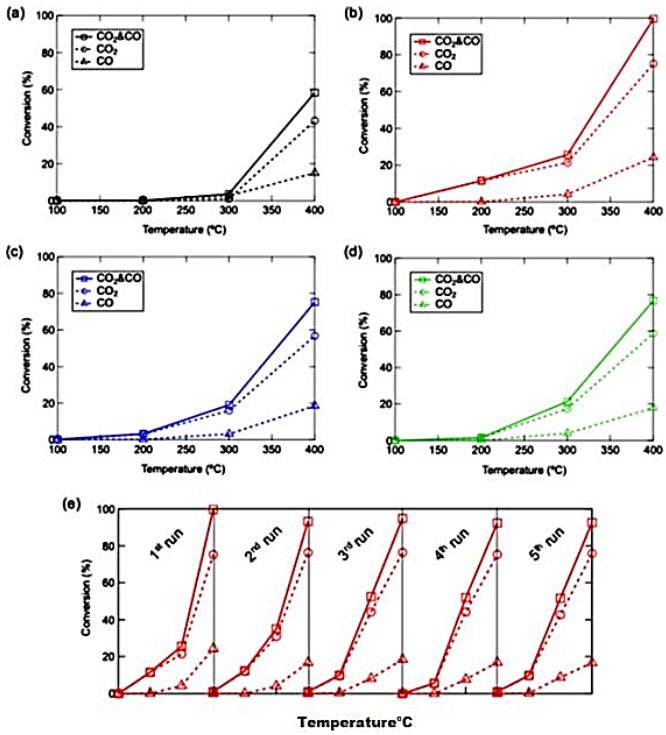

Figure 16. Conversion of CO_2/CO with VOC at elevated temperatures with different materials; (a) raw and mechanochemically activated HAp, (b) 3 mm, (**c**) 10 mm, (d) 15 mm ball, (e) repeatability test of VOC decomposition.[87]

ignored (Figure. 15B). Hence, the treated surface is occupied by active radical, surface basicity, and adsorption affinity can be attributed to more catalytic features with 100 % CO_2/CO conversion for treated HAp (Figure. 16).[87]

LPG Gas Sensing

The sodium doped polycrystalline hydroxyapatite NaHAp (NaOH-HAp) powder by employing wet chemical precipitation method and its composites with alumina (Al_2O_3; 0, 10, 40, 70 wt%) by scalable solid-state technique. The Na-doped HAp and Al_2O_3 compound concentrations ([100-x] NaHAp + xAl_2O_3) (x=0, 10, 40 and 70) were prepared using a mortar and pestle. Further, four different compositions of Na doped HAp and Al_2O_3 composites namely NaHAp, 90H-10A, 60H-40A, and 30H-70A were investigated. The LPG sensor characteristics of the synthesized pure NaHAp material were observed. The variation in the resistance of the NaHAp sample was observed from $3.88x10^6$ to $5.85x10^6$ Ω, from $4.41x10^6$ to $1.07x10^7$ Ω, from $4.95x10^6$ to $2.62x10^7$ Ω and from $5.41x10^6$ to $4.23x10^7$ Ω, respectively, with the exposure of 0.5, 1.0, 1.5 and 2.0 vol.%. The calculated percentage of sensor response for each concentration of the LPG was 50.77, 128.34, 430.91, and 683.18 respectively[77] (Figure. 17). The novel and porous NaHAp-based Al_2O_3 (60H-40A) sensor displays the lowest value of the response time, i.e., 4 s along with 3s recovery time for the 0.5 vol.% concentration of the LPG.[88]

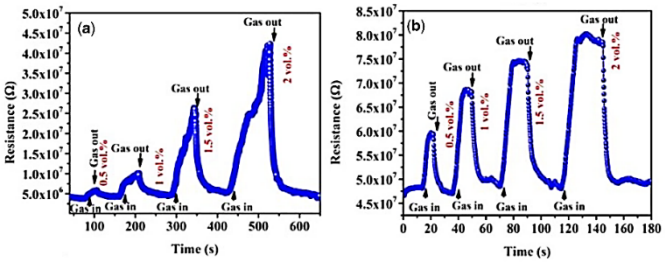

Figure 17. LPG sensing characteristics of composites (a) NaHAp, (b) 90H-10A composite.[88]

Alcohol Vapor Sensing

Furthermore, thick films made of TiO_2 nanotubes (TNT) and HAp nanocomposite were employed to detect alcohol vapors at low temperatures and low concentrations.[89] The screen printing technique used for preparing TNT-HAp nano-composites (Figure. 18A). The pure and nanocomposites morphology was not clearly shown in SEM pictures due to agglomeration. Figure. 18C shows clusters of nanotubes for TNT but composites show no change in morphology (Figure. 18C (c–f)). The elemental study of HAp reveals strong peaks for Ca and P, with a 1.67 ratio, indicating that HAp is stoichiometrically composed. The gas detection process of HAp-TNT nanocomposites is shown in (Figure. 18B(a-b)). The sensitivity factor is increases after alcohol vapor absorption on the surface and saturated with time. HAp and nanocomposite response and recovery times reveal that composites have a faster response and recovery time (Figure. 19). Nanocomposite (HAp-TNt) accompanied with large surface area and more active sites which allows the alcohol detecting by their porous and hollow nanotubes morphology.[89] Improved sensing performance is shown by the TNT substance.[90]

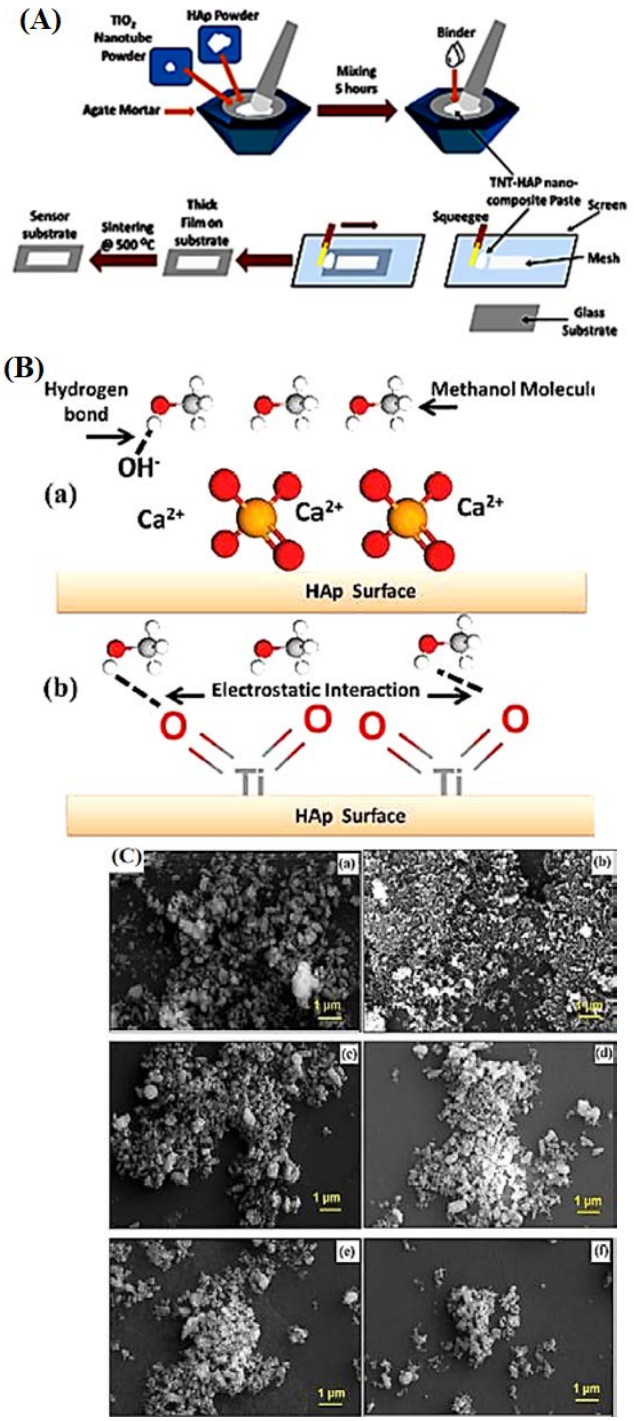

Figure 18. (A) Schematic of HAp-TNT nanocomposite preparation, (B) Representation of surface interaction of HAp and HAp-TNT composites.[90]

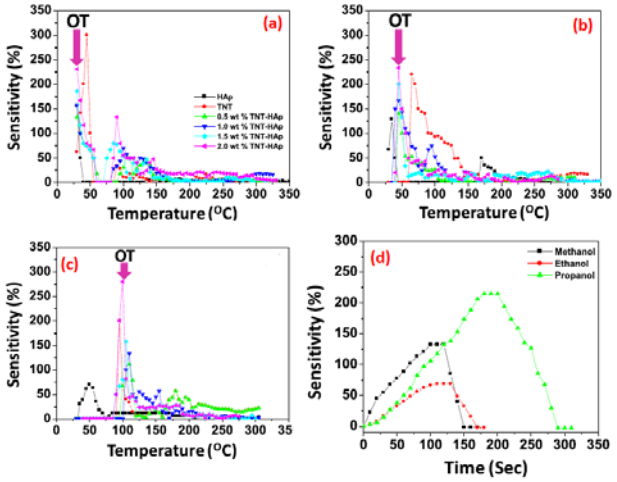

Figure 19. Sensitivity based on temperature with HAp, TNT and TNT-HAp nanocomposites at 10 ppm; (a) methanol, (b) ethanol, (c) propanol vapors, (d) Recovery time of TNT-HAp sensor substrate for methanol, ethanol and propanol vapors at 10 ppm.[90]

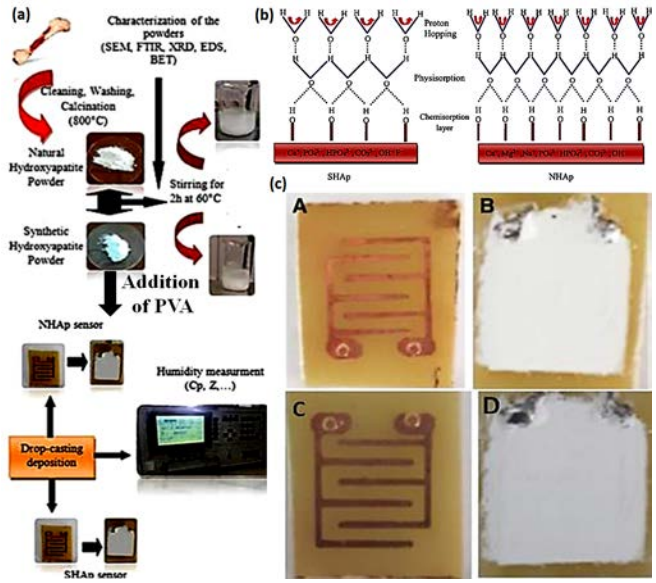

Figure. 20 (a) Synthesis process of NHAp and SHAp, (b) Mechanism of humidity sensing by NHAp and SHAp layers, (c) Pictorial representation of humidity sensors; (A and B) before and after deposition of NHAp, (C and D) before and after deposition of SHAp.[92]

Humidity Sensor

The moisture detection device was constructed by natural induced HAp (NHAp) and synthetically prepared HAp (SHAp) through the sol-gel process and acted as sensitive layers[91] (Figure. 20a). The humidity hysteresis property is determined by the absorption and desorption process. The capacity of this desorption process is slightly lower than that of the adsorption process. The cyclic analysis of the humidity sensor has a tiny hysteresis loop. Equation (9) was used to estimate the relationship of sensitivity and humidity at 16 and 87% at 100 Hz for NHAp and SHAp. In humidity and concentration variation, the NHAp sensitivity varies from 11.42 to 17,900%. The capacity of the SHAp sensor ranges from 4.9 to 47 pF, with sensitivity ranging from 2.17% to 921.73% (Figure. 21).[92]

Aniline Sensor

Researchers have developed a HAp nanorods nano-bio material for extremely efficient aniline detection using quartz crystal microbalance (QCM) transducer.[93] The HAP nanorods have 2

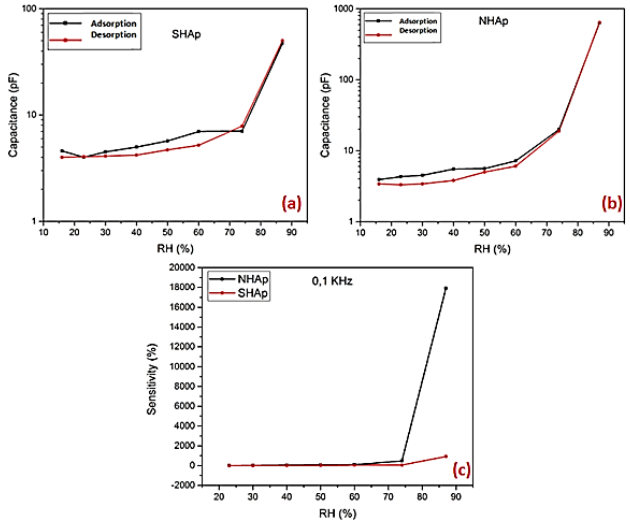

Figure 21. Humidity hysteresis characteristics (a) SHAp, (b) NHAp humidity sensor at 100 Hz, (c) Sensitivity of NHAp and SHAp at 100 Hz.[92]

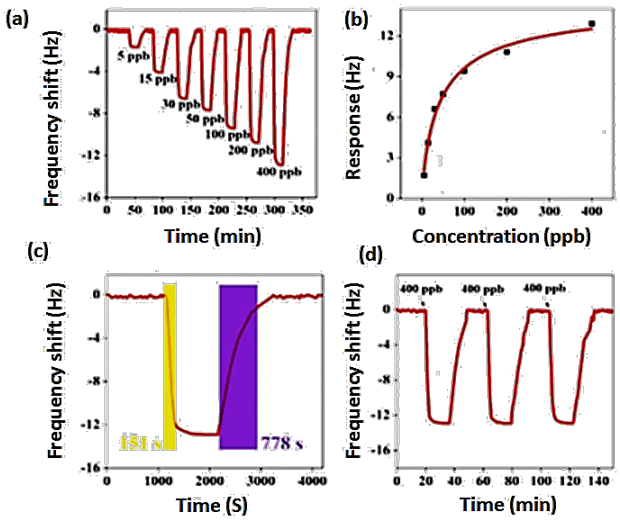

Figure 23. (a and c) Frequency versus time shift of HAP-rod, (b) response curve for aniline vapor with different concentrations, (d) repeatability of HAP at 400 ppb.[94]

acidic ions (hydroxyl and Ca) to detect amino groups in aniline, ensuring sensitivity and selectivity for other gases (Figure. 22A). HAP nanorods were obtained by sol-gel technique with homogeneous structure (Figure. 22B).[99] HAP detects aniline vapor at room temperature to meet the goal of saving energy. The HAp shows an active shift in frequency for aniline vapor detection at varying concentrations from 5 to 400 ppb.[94] The HAp response and recovery curve shows 151 and 778 sec as better sensitivity. In addition, the HAP-repeatability rod shape with aniline vapor is examined. The frequency shift of the HAP with QCM provides good selectivity against other vapors.[95] Furthermore, when compared to pure aniline vapor, the frequency shift toward other vapor is relatively less (Figure. 23). The frequency shift was slightly amplified when aniline was combined with other vapor molecules, is due to the interaction of other vapor molecules upon aniline molecules which adsorbed on HAP surface.[96]

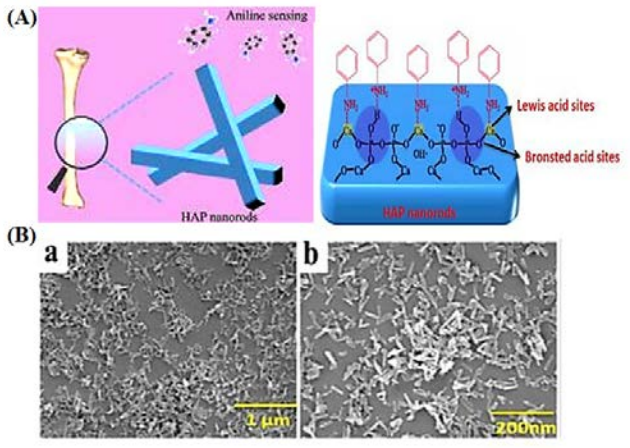

Figure 22. (A) Schematic representation of HAP and aniline sensing mechanism, (B) Morphology of HAP at different magnifications.[94]

Glucose Sensing

The bovine dentin, a natural biomineralized HAp (BioHAP), is used as a hard template in this study, and PANI[97] is polymerized in the template's microtubules to produce a composite. Further for tooth cavity filling silver amalgam (AgHg) is used as a biosensing electrode (PANI-BioHAP/AgHg). The tubules' inner walls are pre-treated with p-methylbenzene sulfonic acid to change their hydrophilic to hydrophobic nature. Meanwhile, the surface of the BioHAP matrix has a significant number of active sites with array shapes for increased glucose electrocatalytic oxidation current responsiveness. The modified electrode prevents Ag from being oxidized to Ag_2O due to its small size and charge transfer process. The two oxidation states show two peaks for PANI from reduction to oxidation state (Figure 24A). The electrochemical degradation of PANI is represented by O5. The oxidation of Ag has three peaks (Figure 24A(b)).[98] When comparing PANI and composites, the

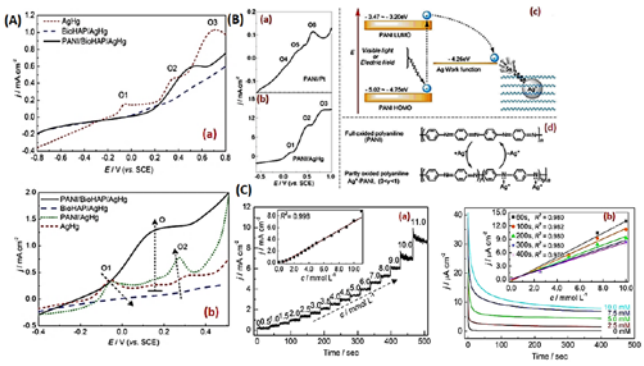

Figure 24. (A)-(a) Voltammetric analysis of AgHg, BioHAP/AgHg and PANI-BioHAP/AgHg electrodes, (b) Voltammetry curve of electrodes with 10 mM glucose; (B) Voltammetric analysis of PANI, AgHg, and composite electrodes; (C) Amperometric analysis of PANI-BioHAP/AgHg electrode for glucose sensing.[99]

Table 2. Sensing properties of different functionalized nHAp materials for gas sensing.

HAp material	Target Gas	Mechanism	Response Time	Gas Uptake Capacity (ppm)	Ref. No.
CNT-HAp	Ethanol	Adsorption/ Desorption	180 s	4500	35
Co, Fe doped HAp	CO	Swift Heavy Ion irradiation (SHI)	30 s	1000	100
Fe doped HAp	CO CO_2	Swift Heavy Ion irradiation (SHI)	25 s 30 s	19,000 16,000	46
TiO_2-HAp nano-composite	Methanol Ethanol Propanol	Ion exchange	130 s 160 s 140 s	2000 1000 900	101
Graphite doped HAp	Methanol Ethanol Propanol	Adsorption/ desorption	90 s 110 s 60 s	50 ppm 50 ppm 50 ppm	6
CNT blended HAp	Methanol	Ion exchange	60 s	100 ppm	102
(Cellulose nanofibrils)-CNF/HAP	Ammonia	Adsorption/ desorption	120 s	900 ppm	103

composites increased by two orders of magnitude, implying that the Ag oxidation peak may obscure the PANI oxidation peak. PANI-BioHAP/AgHg sensing electrode amperometric curve changes with the addition of glucose. The sensing electrode's LoD value for glucose is from 1.0 to 10.0 mM at 0.13 V (Figure. 24C). Compared to AgHg and PANI/AgHg, the current density was increased for PANI-BioHAP/AgHg electrode.[99]

SUMMARY AND FUTURE PERSPECTIVE

In this review, a broad collection of HAp nanocomposite materials-based sensors and their applications in gas sensing were reported. The details and sensing properties of nHAp composite materials used for the detection of various gases through the different methods are presented in Table 2. Furthermore, the recent advances in gas sensing by different HAp nanostructures like a chain, tube, rod, needle, spherical, nano-porous structure, and 3D morphology have been highlighted. The proposed HAp morphology has a significant impact on gas sensing over their conductivity, selectivity, sensitivity, stability, reliability, and repeatability. Interestingly, nano-HAp material and HAp nanocomposites increase the efficiency of gas sensors at optimum temperature conditions. For instance, (i) HAp-graphene and HAp-TiO_2 composite are highly useful for sensing alcohol vapors, acetone, ethanol, and methanol by electrochemical method; (ii) the HAp-CNT composite was also developed for propanol sensing at room temperature with best selectivity and sensitivity; (iii) At room temperatures, the HAp-CNF, HAp-TiO_2, HAp-Au, HAp-PANI used for NH_3 sensing by mechano-chemical method with improved efficiency and reliability at ppm level. The HAp-Ag and HAp-polymer were obtained for glucose sensing through the electrochemical oxidation method with high accuracy. NaHAp and Co-HAp composites were developed using quartz crystal microbalance for LPG, CO_2, and aniline sensing. The bacterial-HAp composite was developed for H_2S gas sensing with enhanced selectivity, stability, and reliability. Hence, the HAp nanostructures and HAP-nanocomposites were established for industrial gas sensing and real-time gas sensing applications. The toxic vapors and their residues in the environment will affect the HAp conductive qualities. Hence, the HAp nanocomposites will be a great candidate for increasing sensitivity in gas detection. The application of new nano-HAp technologies at the molecular scale will upgrade with existing materials, preparation technologies, real-time detection, and controlled morphology which are the primary steps of molecular sensing used for real-time applications with future advances in gas sensing. Furthermore, concerns related to the creation of highly dependable and industrial standard gas sensors for environmental monitoring must be addressed.

CONFLICT OF INTEREST

The authors declare that there are no conflicts of interest concerning this review article.

ACKNOWLEDGMENT

Financial support from the DBT-RA program in Biotechnoiogy and Life Sciences is gratefully acknowledged.

REFERENCES

1. V.N. Narwade, Y.B. Pottathara, S. Begum, et al. Nanostructured hydroxyapatite biomaterial as gas sensor. In *Nanoscale Processing*; Elsevier, **2021**; pp 439–466.
2. B.S. Chhikara, R. Kumar, Poonam, P. Bazard, R.S. Varma. Viral infection mitigations using advanced nanomaterials and tools: lessons from SARS-CoV-2 for future prospective interventions. *J. Mater. Nanosci.* **2021**, 8 (2), 64–82.
3. U. Yaqoob, M.I. Younis. Chemical gas sensors: Recent developments, challenges, and the potential of machine learning—A review. *Sensors* **2021**, 21 (8), 2877.
4. B. Bera. Hydroxyapatite, synthesis of numerous CdS quantum dot composite material: a review. *Int J Nanomater Nanostruct* **2019**, 5, 1–11.
5. Y. Huang, S.S.H. Ho, Y. Lu, et al. Removal of indoor volatile organic compounds via photocatalytic oxidation: a short review and prospect. *Molecules* **2016**, 21 (1), 56.
6. S.R. Anjum, V.N. Narwade, K.A. Bogle, R.S. Khairnar. Graphite doped Hydroxyapatite nanoceramic: Selective alcohol sensor. *Nano-Struct. Nano-Objects* **2018**, 14, 98–105.
7. S.M. Majhi, A. Mirzaei, S. Navale, H.W. Kim, S.S. Kim. Boosting the sensing properties of resistive-based gas sensors by irradiation techniques: a review. *Nanoscale* **2021**, 13 (9), 4728–4757.

8. S. Nakata, T. Arie, S. Akita, K. Takei. Wearable, flexible, and multifunctional healthcare device with an ISFET chemical sensor for simultaneous sweat pH and skin temperature monitoring. *ACS Sens.* **2017**, 2 (3), 443–448.
9. S. Bodhak, S. Bose, A. Bandyopadhyay. Influence of MgO, SrO, and ZnO dopants on electro-thermal polarization behavior and in vitro biological properties of hydroxyapatite ceramics. *J. Am. Ceram. Soc.* **2011**, 94 (4), 1281–1288.
10. V. Saxena, A. Hasan, L.M. Pandey. Effect of Zn/ZnO integration with hydroxyapatite: a review. *Mater. Technol.* **2018**, 33 (2), 79–92.
11. S.-I. Jinga, A.-I. Zamfirescu, G. Voicu, et al. PCL-ZnO/TiO2/HAp electrospun composite fibers with applications in tissue engineering. *Polymers* **2019**, 11 (11), 1793.
12. K. Naik, V.G. Chandran, R. Rajashekaran, S. Waigaonkar, M. Kowshik. Mechanical properties, biological behaviour and drug release capability of nano TiO2-HAp-Alginate composite scaffolds for potential application as bone implant material. *J. Biomater. Appl.* **2016**, 31 (3), 387–399.
13. M.U.A. Khan, S. Haider, S.A. Shah, et al. Arabinoxylan-co-AA/HAp/TiO2 nanocomposite scaffold a potential material for bone tissue engineering: An in vitro study. *Int. J. Biol. Macromol.* **2020**, 151, 584–594.
14. Y. Yan, X. Zhang, H. Mao, et al. Hydroxyapatite/gelatin functionalized graphene oxide composite coatings deposited on TiO2 nanotube by electrochemical deposition for biomedical applications. *Appl. Surf. Sci.* **2015**, 329, 76–82.
15. C.M. Magdalane, K. Kanimozhi, M.V. Arularasu, G. Ramalingam, K. Kaviyarasu. Self-cleaning mechanism of synthesized SnO2/TiO2 nanostructure for photocatalytic activity application for wastewater treatment. *Surf. Interfaces* **2019**, 17, 100346.
16. R. Shiwaku, H. Matsui, K. Nagamine, et al. A printed organic circuit system for wearable amperometric electrochemical sensors. *Sci. Rep.* **2018**, 8 (1), 1–8.
17. M.N. Padvi, A.V. Moholkar, S.R. Prasad, N.R. Prasad. A critical review on design and development of gas sensing materials. *Eng. Sci.* **2021**, 15, 20–37.
18. S.B. Kondawar, A.M. More, H.J. Sharma, S.P. Dongre. Ag-SnO2/Polyaniline composite nanofibers for low operating temperature hydrogen gas sensor. *J. Mater. Nanosci.* **2017**, 4 (1), 13–18.
19. P.D. Virutkar, A.P. Mahajan, B.H. Meshram, S.B. Kondawar. Conductive polymer nanocomposite enzyme immobilized biosensor for pesticide detection. *J. Mater. Nanosci.* **2019**, 6 (1), 7–12.
20. A. Dahiya, S.L. Goyal, D. Jain, N. Kishore. Synthesis and Fourier Transform Infra-Red Spectroscopy of Polyaniline/Cobalt Chloride Composites. *J. Integr. Sci. Technol.* **2017**, 5 (2), 47–49.
21. Q. Zhou, W. Chen, L. Xu, et al. Highly sensitive carbon monoxide (CO) gas sensors based on Ni and Zn doped SnO2 nanomaterials. *Ceram. Int.* **2018**, 44 (4), 4392–4399.
22. V.S. Rizi, F. Sharifianjazi, H. Jafarikhorami, et al. Sol-gel derived SnO2/Ag2O ceramic nanocomposite for H2 gas sensing applications. *Mater. Res. Express* **2019**, 6 (11), 1150g2.
23. X. Tong, W. Shen, X. Chen. Enhanced H2S sensing performance of cobalt doped free-standing TiO2 nanotube array film and theoretical simulation based on density functional theory. *Appl. Surf. Sci.* **2019**, 469, 414–422.
24. X.-T. Yin, W.-D. Zhou, J. Li, et al. Tin dioxide nanoparticles with high sensitivity and selectivity for gas sensors at sub-ppm level of hydrogen gas detection. *J. Mater. Sci. Mater. Electron.* **2019**, 30 (15), 14687–14694.
25. X. Liu, S. Cheng, H. Liu, et al. A survey on gas sensing technology. *Sensors* **2012**, 12 (7), 9635–9665.
26. G. Radha, B. Venkatesan, S.N. Jaisankar, P. Rajashree, S. Balakumar. Interplay between surface chemistry and osteogenic behaviour of sulphate substituted nano-hydroxyapatite. *Mater. Sci. Eng. C* **2021**, 120.
27. D. Sivaraj, K. Vijayalakshmi. Substantial effect of magnesium incorporation on hydroxyapatite/carbon nanotubes coatings on metallic implant surfaces for better anticorrosive protection and antibacterial ability. *J. Anal. Appl. Pyrolysis* **2018**, 135, 15–21.
28. G. Radha, B. Venkatesan, P. Rajashree, E. Vellaichamy, S. Balakumar. Insights into the apatite mineralization potential of thermally processed nanocrystalline Ca10-xFex(PO4)6(OH)2. *New J. Chem.* **2019**, 43 (3), 1358–1371.
29. D. Sivaraj, K. Vijayalakshmi. Enhanced antibacterial and corrosion resistance properties of Ag substituted hydroxyapatite/functionalized multiwall carbon nanotube nanocomposite coating on 316L stainless steel for biomedical application. *Ultrason. Sonochem.* **2019**, 59, 104730.
30. G. Radha, B. Venkatesan, E. Vellaichamy, S. Balakumar. Structural, Mechanical and Biological Insights on Reduced Graphene Nanosheets Reinforced Sonochemically Processed Nano-Hydroxyapatite Ceramics. *Ceram. Int.* **2018**, 44 (8), 8777–8787.
31. D. Sivaraj, K. Vijayalakshmi, A. Ganeshkumar, R. Rajaram. Tailoring Cu substituted hydroxyapatite/functionalized multiwalled carbon nanotube composite coating on 316L SS implant for enhanced corrosion resistance, antibacterial and bioactive properties. *Int. J. Pharm.* **2020**, 590, 119946.
32. G. Radha, S. Balakumar, B. Venkatesan, E. Vellaichamy. A novel nano-hydroxyapatite—PMMA hybrid scaffolds adopted by conjugated thermal induced phase separation (TIPS) and wet-chemical approach: Analysis of its mechanical and biological properties. *Mater. Sci. Eng. C* **2017**, 75, 221–228.
33. S. Pai, S.M. Kini, R. Selvaraj, A. Pugazhendhi. A review on the synthesis of hydroxyapatite, its composites and adsorptive removal of pollutants from wastewater. *J. Water Process Eng.* **2020**, 38, 101574.
34. A. Fihri, C. Len, R.S. Varma, A. Solhy. Hydroxyapatite: A review of syntheses, structure and applications in heterogeneous catalysis. *Coord. Chem. Rev.* **2017**, 347, 48–76.
35. R.S. Khairnar, S.R. Anjum, M.P. Mahabole. Development of CNT doped nano-HAp thick film gas sensor. *Development* **2014**, 3 (3), 253–261.
36. M.P. Mahabole, R.U. Mene, R.S. Khairnar. Gas sensing and dielectric studies on cobalt-doped hydroxyapatite thick films. *Gas* **2013**, 900 (1), 46–52.
37. R.S. Khairnar, R.U. Mene, S.G. Munde, M.P. Mahabole. Nano-hydroxyapatite thick film gas sensors. In *AIP Conference Proceedings*; American Institute of Physics, **2011**; Vol. 1415, pp 189–192.
38. R.S. Khairnar, S.R. Anjum, V. Kokol, M.P. Mahabole. Carbon nanotube doped nano-hydroxyapatite sensor matrix for gas sensing application. *Int. J. Mod. Commun. Technol. Res.* **2014**, 2 (4), 29–34.
39. C.R. Bowen, J. Gittings, I.G. Turner, F. Baxter, J.B. Chaudhuri. Dielectric and piezoelectric properties of hydroxyapatite-Ba Ti O 3 composites. *Appl. Phys. Lett.* **2006**, 89 (13), 132906.
40. S. Nakamura, H. Takeda, K. Yamashita. Proton transport polarization and depolarization of hydroxyapatite ceramics. *J. Appl. Phys.* **2001**, 89 (10), 5386–5392.
41. P. Malmberg, H. Nygren. Methods for the analysis of the composition of bone tissue, with a focus on imaging mass spectrometry (TOF-SIMS). *Proteomics* **2008**, 8 (18), 3755–3762.
42. R.G. Carrodeguas, S. De Aza. α-Tricalcium phosphate: Synthesis, properties and biomedical applications. *Acta Biomater.* **2011**, 7 (10), 3536–3546.
43. A. Chetty, I. Wepener, M.K. Marei, Y.E. Kamary, R.M. Moussa. Synthesis, properties, and applications of hydroxyapatite; Nova Science Publishers, **2012**.
44. M.P. Mahabole, R.C. Aiyer, C.V. Ramakrishna, B. Sreedhar, R.S. Khairnar. Synthesis, characterization and gas sensing property of hydroxyapatite ceramic. *Bull. Mater. Sci.* **2005**, 28 (6), 535–545.
45. S. Sōmiya, R. Roy. Hydrothermal synthesis of fine oxide powders. *Bull. Mater. Sci.* **2000**, 23 (6), 453–460.
46. R.U. Mene, M.P. Mahabole, K.C. Mohite, R.S. Khairnar. Improved gas sensing and dielectric properties of Fe doped hydroxyapatite thick films: Effect of molar concentrations. *Mater. Res. Bull.* **2014**, 50, 227–234.
47. A. Bianco, I. Cacciotti, M. Lombardi, L. Montanaro. Si-substituted hydroxyapatite nanopowders: synthesis, thermal stability and sinterability. *Mater. Res. Bull.* **2009**, 44 (2), 345–354.

48. L. Medveckỳ, R. Štulajterová, L. Parilák, et al. Influence of manganese on stability and particle growth of hydroxyapatite in simulated body fluid. *Colloids Surf. Physicochem. Eng. Asp.* **2006**, 281 (1–3), 221–229.
49. L. Huixia, L. Yong, L. Lanlan, et al. Development of ammonia sensors by using conductive polymer/hydroxyapatite composite materials. *Mater. Sci. Eng. C* **2016**, 59, 438–444.
50. A. Afzal, A. Mujahid, N. Iqbal, R. Javaid, U.Y. Qazi. Enhanced high-temperature (600° C) NO2 response of ZnFe2O4 nanoparticle-based exhaust gas sensors. *Nanomaterials* **2020**, 10 (11), 2133.
51. J.A. Jarmoshti, A. Nikfarjam, H. Hajghassem, S.M. Banihashemian. Visible light enhancement of ammonia detection using silver nanoparticles decorated on reduced graphene oxide. *Mater. Res. Express* **2019**, 6 (6), 066306.
52. D. Acharyya, N. Banerjee, P. Bhattacharyya. A comparative study on methanol sensing performance of ZnO nanoflower and nanorod based resistive devices. In *SENSORS, 2014 IEEE*; IEEE, **2014**; pp 811–814.
53. F. Hossein-Babaei, M. Keshmiri, M. Kakavand, T. Troczynski. A resistive gas sensor based on undoped p-type anatase. *Sens. Actuators B Chem.* **2005**, 110 (1), 28–35.
54. M. Tonezzer. Selective gas sensor based on one single SnO2 nanowire. *Sens. Actuators B Chem.* **2019**, 288, 53–59.
55. F. Zhang, A. Zhu, Y. Luo, et al. CuO nanosheets for sensitive and selective determination of H2S with high recovery ability. *J. Phys. Chem. C* **2010**, 114 (45), 19214–19219.
56. R.U. Mene, M.P. Mahabole, R.S. Khairnar. Surface modified hydroxyapatite thick films for CO2 gas sensing application: Effect of swift heavy ion irradiation. *Radiat. Phys. Chem.* **2011**, 80 (6), 682–687.
57. L. Luo, Y. Liu, Y. Tan, et al. Room temperature gas sensor based on tube-like hydroxyapatite modified with gold nanoparticles. *J. Cent. South Univ.* **2016**, 23 (1), 18–26.
58. S.C. Hernandez, D. Chaudhuri, W. Chen, N.V. Myung, A. Mulchandani. Single polypyrrole nanowire ammonia gas sensor. *Electroanal. Int. J. Devoted Fundam. Pract. Asp. Electroanal.* **2007**, 19 (19–20), 2125–2130.
59. A.L. Kukla, Y.M. Shirshov, S.A. Piletsky. Ammonia sensors based on sensitive polyaniline films. *Sens. Actuators B Chem.* **1996**, 37 (3), 135–140.
60. Y. Zhang, K. Li, Q. Zhang, et al. Multi-dimensional hydroxyapatite (HAp) nanocluster architectures fabricated via Nafion-assisted biomineralization. *New J. Chem.* **2015**, 39 (1), 750–754.
61. J. Gong, Y. Li, Z. Hu, Z. Zhou, Y. Deng. Ultrasensitive NH3 gas sensor from polyaniline nanograin enchased TiO2 fibers. *J. Phys. Chem. C* **2010**, 114 (21), 9970–9974.
62. Y. Zhang, Y. Liu, X. Ji, C.E. Banks, W. Zhang. Sea cucumber-like hydroxyapatite: cation exchange membrane-assisted synthesis and its application in ultra-sensitive heavy metal detection. *Chem. Commun.* **2011**, 47 (14), 4126–4128.
63. D. Zhang, J. Liu, C. Jiang, A. Liu, B. Xia. Quantitative detection of formaldehyde and ammonia gas via metal oxide-modified graphene-based sensor array combining with neural network model. *Sens. Actuators B Chem.* **2017**, 240, 55–65.
64. M. Sun, Z. Li, Y. Gu, S. Wu, X. Wang. Room-temperature high-performance ammonia gas sensor based on hydroxyapatite film. *Mater. Res. Express* **2019**, 6 (10), 106401.
65. H. Ye, X.Y. Liu, H. Hong. Characterization of sintered titanium/hydroxyapatite biocomposite using FTIR spectroscopy. *J. Mater. Sci. Mater. Med.* **2009**, 20 (4), 843–850.
66. S.W. Chen, O.K. Khor, M.W. Liao, C.K. Chung. Sensitivity evolution and enhancement mechanism of porous anodic aluminum oxide humidity sensor using magnetic field. *Sens. Actuators B Chem.* **2014**, 199, 384–388.
67. J. Zhu. Photocatalytic properties of thin films of ruthenium metallopolymers/gold nanoparticle: Polyoxometalate composites using visible excitation. *J. Cent. South Univ.* **2013**, 20 (10), 2657–2662.
68. A. Dufresne. Nanocellulose: a new ageless bionanomaterial. *Mater. Today* **2013**, 16 (6), 220–227.
69. M.R.K. Sofla, R.J. Brown, T. Tsuzuki, T.J. Rainey. A comparison of cellulose nanocrystals and cellulose nanofibres extracted from bagasse using acid and ball milling methods. *Adv. Nat. Sci. Nanosci. Nanotechnol.* **2016**, 7 (3), 035004.
70. J.V. Edwards, N. Prevost, A. French, et al. Nanocellulose-based biosensors: Design, preparation, and activity of peptide-linked cotton cellulose nanocrystals having fluorimetric and colorimetric elastase detection sensitivity. **2013**.
71. V.N. Narwade, S.R. Anjum, V. Kokol, R.S. Khairnar. Ammonia-sensing ability of differently structured hydroxyapatite blended cellulose nanofibril composite films. *Cellulose* **2019**, 26 (5), 3325–3337.
72. M.J. Allen, V.C. Tung, R.B. Kaner. Honeycomb carbon: a review of graphene. *Chem. Rev.* **2010**, 110 (1), 132–145.
73. Q. Zhang, Y. Liu, Y. Zhang, et al. Facile and controllable synthesis of hydroxyapatite/graphene hybrid materials with enhanced sensing performance towards ammonia. *Analyst* **2015**, 140 (15), 5235–5242.
74. L. Gu, K. Zheng, Y. Zhou, et al. Humidity sensors based on ZnO/TiO2 core/shell nanorod arrays with enhanced sensitivity. *Sens. Actuators B Chem.* **2011**, 159 (1), 1–7.
75. S. Taha, V.N. Narwade, S.R. Anjum, et al. Nano-TiO2 doped hydroxyapatite nanoceramics: development of ammonia sensor. In *IJCAR*; **2018**; Vol. 7, pp 11069–11074.
76. L. Huixia, L. Yong, T. Yanni, et al. Room temperature gas sensing properties of tubular hydroxyapatite. *New J. Chem.* **2015**, 39 (5), 3865–3874.
77. K. Igarashi, M. Takiguchi, H. Ooshima. Growth mechanism of the calcium carbonate tubes on a cation-exchange membrane. *J. Ceram. Soc. Jpn.* **2008**, 116 (1349), 111–114.
78. D.R. Patil, L.A. Patil, P.P. Patil. Cr2O3-activated ZnO thick film resistors for ammonia gas sensing operable at room temperature. *Sens. Actuators B Chem.* **2007**, 126 (2), 368–374.
79. Y. Wang, S. Wang, Y. Zhao, et al. H2S sensing characteristics of Pt-doped α-Fe2O3 thick film sensors. *Sens. Actuators B Chem.* **2007**, 125 (1), 79–84.
80. M.V. Vaishampayan, R.G. Deshmukh, P. Walke, I.S. Mulla. Fe-doped SnO2 nanomaterial: A low temperature hydrogen sulfide gas sensor. *Mater. Chem. Phys.* **2008**, 109 (2–3), 230–234.
81. J. Daoud, D. Karamanev. Formation of jarosite during Fe2+ oxidation by Acidithiobacillus ferrooxidans. *Miner. Eng.* **2006**, 19 (9), 960–967.
82. Z. Xu, J. Liang, L. Zhou. Photo-Fenton-like degradation of azo dye methyl orange using synthetic ammonium and hydronium jarosite. *J. Alloys Compd.* **2013**, 546, 112–118.
83. Y. Tan, H. Li, Y. Liu, et al. Acidithiobacillus ferrooxidans improved H 2 S gas sensing properties of tubular hydroxyapatite at room temperature. *RSC Adv.* **2016**, 6 (80), 76874–76878.
84. R.U. Mene, M.P. Mahabole, R.S. Khairnar. P1. 9.9 Surface Modification of Cobalt doped Hydroxyapatite Thick Films via Swift Heavy Ion Irradiations for CO and CO2 Gas Sensing Application. *Proc. IMCS 2012* **2012**, 1180–1183.
85. Y. Guo, M. Wen, G. Li, T. An. Recent advances in VOC elimination by catalytic oxidation technology onto various nanoparticles catalysts: a critical review. *Appl. Catal. B Environ.* **2021**, 281, 119447.
86. S. Song, S. Zhang, X. Zhang, P. Verma, M. Wen. Advances in catalytic oxidation of volatile organic compounds over Pd-supported catalysts: recent trends and challenges. *Front. Mater.* **2020**, 342.
87. Y. Xin, T. Shirai. Noble-metal-free hydroxyapatite activated by facile mechanochemical treatment towards highly-efficient catalytic oxidation of volatile organic compound. *Sci. Rep.* **2021**, 11 (1), 1–13.
88. S.K. Avinashi, A. Hussain, K. Kumar, B.C. Yadav, C. Gautam. Synthesis and structural characterizations of HAp–NaOH–Al2O3 composites for liquid petroleum gas sensing applications. *Oxf. Open Mater. Sci.* **2021**, 1 (1), itab006.
89. M. Shooshtari, A. Salehi, S. Vollebregt. Effect of temperature and humidity on the sensing performance of TiO2 nanowire-based ethanol vapor sensors. *Nanotechnology* **2021**, 32 (32), 325501.

90. S. Taha, S. Begum, V.N. Narwade, et al. Enhancing alcohol sensing properties of hydroxyapatite via synthesis of its composite with TiO2 nanotube. *Appl. Phys. A* **2021**, 127 (7), 1–9.
91. T. Julian, A. Rianjanu, S.N. Hidayat, et al. Quartz crystal microbalance coated with PEDOT–PSS/PVA nanofiber for a high-performance humidity sensor. *J. Sens. Sens. Syst.* **2019**, 8 (2), 243–250.
92. L. Khtaoui, M. Laghrouche, F. Fernane, A. Chaouchi. High-sensitivity humidity sensor based on natural hydroxyapatite. *J. Mater. Sci. Mater. Electron.* **2021**, 32 (7), 8668–8686.
93. N.L. Torad, S. Zhang, W.A. Amer, et al. Advanced nanoporous material–based QCM devices: A new horizon of interfacial mass sensing technology. *Adv. Mater. Interfaces* **2019**, 6 (20), 1900849.
94. L. Wang, B. Wang, Y. Wu, J. Song. Hydroxyapatite nanorods: a nano biomaterials for chemical detection of aniline vapor. *J. Iran. Chem. Soc.* **2022**, 19 (1), 211–218.
95. X. Hu, C. Wang, R. Luo, et al. Double-shelled hollow ZnO/carbon nanocubes as an efficient solid-phase microextraction coating for the extraction of broad-spectrum pollutants. *Nanoscale* **2019**, 11 (6), 2805–2811.
96. M. Ibrahim, M. Labaki, J.-M. Giraudon, J.-F. Lamonier. Hydroxyapatite, a multifunctional material for air, water and soil pollution control: A review. *J. Hazard. Mater.* **2020**, 383, 121139.
97. J. Wang, Y. Ning, Y. Wen, et al. Characteristics and electrochemical reaction kinetics of polyaniline nanofibers as a promoter of Pt electrode for methanol electrocatalytic oxidation. *Z. Für Phys. Chem.* **2013**, 227 (1), 89–104.
98. A. Dhillon, S. Prasad, D. Kumar. Recent advances and spectroscopic perspectives in fluoride removal. *Appl. Spectrosc. Rev.* **2017**, 52 (3), 175–230.
99. Y. Jiang, H. Liu, X. Qi, et al. Conductive Ag-Based Modification of Hydroxyapatite Microtubule Array and Its Application to Enzyme-Free Glucose Sensing. *ChemistrySelect* **2018**, 3 (9), 2542–2547.
100. R.U. Mene, M.P. Mahabole, K.C. Mohite, R.S. Khairnar. Fe doped hydroxyapatite thick films modified via swift heavy ion irradiation for CO and CO2 gas sensing application. *J. Alloys Compd.* **2014**, 584, 487–493.
101. S. Taha, S. Begum, V.N. Narwade, et al. Development of alcohol sensor using TiO2-Hydroxyapatite nano-composites. *Mater. Chem. Phys.* **2020**, 240, 122228.
102. S.R. Anjum, R.S. Khairnar. Integrated Sensing of Alcohols by CNT Blended HAp Nano Ceramics. *Sens. Transducers* **2016**, 206 (11), 1.
103. V.N. Narwade, K.A. Bogle, V. Kokol. Hydrothermally synthesized hydroxyapatite cellulose composites thick films as ammonia gas sensor. *Emergent Mater.* **2021**, 1–10.

AUTHORS BIOGRAPHIES

Dr. N. Manjubaashini received her Bachelor of Engineering and Master of Technology degrees from Anna University, India, in 2012 and 2014, respectively. She was a Senior Research Fellow in the Council of Scientific and Industrial Research grants program when she earned her Ph.D. in Technology from Anna University, India, in 2019. Currently works as a Research Associate under the Department of Bio-Technology scheme at the National Centre for Nanoscience and Nanotechnology, University of Madras, Chennai, India. Her research focuses on the synthesis of metal-based nanomaterials and bioactive materials used in healthcare and environmental restoration.

Dr. G. Radha, ICMR-RA in National Centre for Nanoscience and Nanotechnology, University of Madras, Chennai, India. Her research interest is bioactive implant coatings, drug delivery systems, nano biomaterials, and polymer-based nanostructures for biomedical applications. She did Ph.D. in Nano-hydroxyapatite for Orthopaedic and Dental Applications at the University of Madras. She is a recipient of the UGC-Rajiv Gandhi National Fellowship and Best Thesis Award for significant research publications on Doctoral research. She has published several research articles in high-quality peer-reviewed international journals. Currently, she is working in nanobiomaterials for cancer treatment.

Prof. S. Balakumar, Director for National Centre for Nanoscience and Nanotechnology; Chairman for School of Nanoscience and Photonics, Coordinator MHRD-GIANT programme, University of Madras, Chennai, India. Eminent Researcher with several Awards and Honors from various Government Funding Agencies. Principal Invigilator for various projects under DST, DBT, ICMR, BIRAC, and TANSCHE. NSTB Post-doctoral Fellow from the National University of Singapore. His research interest is Biomedical Nanotechnology, Nanomaterials for Energy and Environment Clean, Environment, Sensing and Storage applications, Nanoelectronics and Nanomagnetism, Biomaterials for orthopedic, dentistry, and ophthalmology.